AIP | The Journal of Chemical Physics

Localization and dynamical arrest of colloidal fluids in a disordered matrix of polydisperse obstacles

Luis Fernando Elizondo-Aguilera and Magdaleno Medina-Noyola

Citation: The Journal of Chemical Physics **142**, 224901 (2015); doi: 10.1063/1.4922155
View online: http://dx.doi.org/10.1063/1.4922155
View Table of Contents: http://scitation.aip.org/content/aip/journal/jcp/142/22?ver=pdfcov
Published by the AIP Publishing

Localization and dynamical arrest of colloidal fluids in a disordered matrix of polydisperse obstacles

Luis Fernando Elizondo-Aguilera[1,a)] and Magdaleno Medina-Noyola[2]
[1]*Facultad de Ciencias Físico-Matemáticas, Benemérita Universidad Autónoma de Puebla, Apartado Postal 1152, 72000 Puebla, PUE., México*
[2]*Instituto de Física Manuel Sandoval Vallarta, Universidad Autónoma de San Luis Potosí, Alvaro Obregón 64, 78000 San Luis Potosí, SLP, Mexico*

(Received 10 March 2015; accepted 26 May 2015; published online 8 June 2015)

The mobility of a colloidal particle in a crowded and confined environment may be severely reduced by its interactions with other mobile colloidal particles and the fixed obstacles through which it diffuses. The latter may be modelled as an array of obstacles with random fixed positions. In this contribution, we report on the effects of the size-polydispersity of such fixed obstacles on the immobilization and dynamical arrest of the diffusing colloidal particles. This complex system is modelled as a monodisperse Brownian hard-sphere fluid diffusing through a polydisperse matrix of fixed hard spheres with a given size distribution. In the Lorentz gas limit (absence of interactions between the mobile particles), we first develop a simple excluded-volume theory to describe the localization transition of the tracer mobile particles. To take into account the interactions among the mobile particles, we adapt the multi-component self-consistent generalized Langevin equation (SCGLE) theory of colloid dynamics, which also allows us to calculate the dynamical arrest transition line, and in general, all the dynamical properties of the mobile particles (mean-squared displacement, self-diffusion coefficient, etc.). The scenarios described by both approaches in the Lorentz gas limit are qualitatively consistent, but the SCGLE formalism describes the dependence of the dynamics of the adsorbed fluid on the polydispersity of the porous matrix at arbitrary concentrations of the mobile spheres and arbitrary volume fractions of the obstacles. Two mechanisms for dynamical arrest (glass transition and localization) are analyzed and we also discuss the crossover between them using the SCGLEs. © *2015 AIP Publishing LLC.* [http://dx.doi.org/10.1063/1.4922155]

I. INTRODUCTION

A large number of experimentally important conditions, ranging from biological systems (proteins diffusing in the cell's cytoplasm or cells transported in capillaries[1–4]) to nano- and micro-structured materials (diffusion of molecular probes through nano-sized porous media[5,6]), require the understanding of the diffusion of molecular, macromolecular, or colloidal probes through crowded environments and within restrictive confining spaces.[7,8] This defines a general problem of considerable fundamental and practical relevance, namely, understanding the dependence of the mobility of such tracer particles on the interactions between them (leading to congested motion even in the absence of confinement) and with the confining medium (which may also impair the mobility of the tracer particles even in the absence of interactions between them).[9,10] One particular aspect of this general problem refers to the description of the competing influence of the severity of the confinement and of the degree of crowding, each of which might lead to the immobilization of the diffusing probes.[11–16]

Thus, it is desirable to develop approaches that simultaneously describe the influence of these two effects on the conditions for immobilization in terms of simple models[17,18] and theories.[13,14] Given the large number of possible specific conditions, it is also desirable to focus on generic but still simple models that mimic the essential features of these otherwise complex phenomena. One such generic model consists of a random array of fixed obstacles that represent a porous matrix as the confining geometry and a set of mobile particles that diffuse through the free space left available, which may represent an adsorbed colloidal fluid. The description of the exact conditions that give rise to localization and trapping of colloidal probes under this type of confinement may be simplified by modelling both, porous matrix and diffusing probes, as collections of hard-spheres (HS). The slow dynamics of the adsorbed hard sphere fluid in the presence of immobile HS obstacles of the same size was investigated by Krakoviack[13,14] using the replica mode-coupling theory (RMCT) that he developed for this purpose. The same problem has also been addressed with the assistance of molecular dynamics simulations.[15,16] Beyond these pioneering works, there has been a recent renewed interest in the so-called *partially pinned* (PP) systems, which may be conceptually described as fluids in which some of the particles (randomly selected from an equilibrium configuration) are positionally frozen.[19,20] Thus, further studies have been performed to investigate the effects of a random pinning field on the static and dynamic properties of thermalized dense fluids.[21–25]

a)luisfer.elizondo@gmail.com

In any of the aforementioned works, however, the effects of the polydispersity of the matrix of obstacles have been reported and thus starting from the same kind of model, the general aim of the present work also consists in determining the influence of both crowding and interactions between the mobile particles on the immobilization of the latter. Our specific goal, however, is to characterize the effects of the size-polydispersity of the fixed obstacles on the diffusion properties of the mobile species and on the dynamical arrest phenomena by means of an alternative theoretical approach to that of Krakoviack. Although we shall consider the simultaneous influence of both, confinement and crowding, in a first stage, we focus only on the effects of confinement, in the absence of interactions between the mobile particles. For this, we discuss the limit of zero-density of mobile particles, sometimes referred to as the *Lorentz gas*[26–28] limit, which allows us to develop a simple free-volume theory to describe the effects of the polydispersity of the matrix on the localization threshold of the mobile probes. In the opposite limit (large density of the adsorbed fluid), the diffusivity of the mobile particles is simultaneously affected by the confinement and by the direct interactions between them. To take into account both effects, in this work, we shall rely on the adaptation of the Self-consistent Generalized Langevin Equation (SCGLE) theory of colloid dynamics[29–31] for equilibrated mixtures, in which we artificially set to zero the mobility of some of the particles (to model the porous matrix), while the other species, which represents the adsorbed fluid, remains mobile. This approach, which follows previous work of our group,[32] will allow us to obtain the dynamical arrest transition line[33,34] and to describe the influence of the size polydispersity of the obstacles on the kinetic arrest phenomena. As it will be shown below, the predictions of the excluded volume theory (EVT) proposed in the first part of the paper are qualitatively consistent with those obtained with the SCGLE theory, regarding the dependence of the percolation threshold on the degree of polydispersity of the matrix. As an additional bonus, however, the SCGLE theory is able to calculate dynamical properties such as the mean square displacement (MSD) $\langle(\Delta\mathbf{r}(t))^2\rangle$, and/or the self-intermediate scattering function (self-ISF) $F^{(s)}(k,t) \equiv \langle \exp[i\mathbf{k}\cdot\Delta\mathbf{r}(t)]\rangle$, of the adsorbed colloidal fluid.

This paper is organized as follows: in Sec. II, we define the general model system considered and then restrict ourselves to the *Lorentz gas* limit in order to introduce our EVT that describes the dependence of the percolation threshold on the size-polydispersity of the porous matrix. In Sec. III, we summarize the SCGLE theory of dynamic arrest and discuss how to use it to describe localization in random porous media. We then establish the qualitative consistency between the predictions of our EV model and the results of the SCGLE theory in the Lorentz gas limit. In Sec. IV, we extend the use of the SCGLE theory to simultaneously describe confinement, crowding, and polydispersity effects, presenting the results in terms of illustrative dynamical arrest diagrams. In Sec. V, we present and discuss our theoretical predictions for the dynamical properties of the embedded fluid. Finally, in Sec. VI, we summarize our main conclusions.

II. COLLOIDAL FLUID ADSORBED IN A RANDOM POROUS MATRIX

Let us start by considering a model system, formed by a set of $N^{(f)}$ hard spheres *fixed* in space in a disordered configuration inside a volume V and constituting our porous matrix. In the portion of the volume left available by this porous matrix, we accommodate other $N^{(m)}$ *mobile* hard-spheres of diameter $\sigma^{(m)}$, which constitute the adsorbed *monodisperse* Brownian fluid.[35] In the present work, we wish to study the dependence of the dynamics of this adsorbed fluid on the size-polydispersity of the fixed obstacles. For this, we assume that each of the $N^{(f)}$ fixed hard-spheres belong to one of ν_f species that differ only in the diameters, $\sigma_1^{(f)}$, $\sigma_2^{(f)},\ldots,\sigma_{\nu_f}^{(f)}$, and in the corresponding number densities, $n_i^{(f)} \equiv N_i^{(f)}/V$. Thus, we define the volume fraction occupied by these fixed particles as $\phi^{(f)} \equiv V^{-1}\sum_{i=1}^{\nu_f} N_i^{(f)}\left[\frac{4}{3}\pi\left(\frac{\sigma_i^{(f)}}{2}\right)^3\right]$, which can also be written, denoting by $n^{(f)}$ $(\equiv\sum_{i=1}^{\nu_f} n_i^{(f)})$ the *total* number density of obstacles, as

$$\phi^{(f)} = \frac{\pi}{6} n^{(f)} \overline{\left[\sigma^{(f)}\right]^3}, \tag{1}$$

where $\overline{\left[\sigma^{(f)}\right]^3} \equiv \sum_{i=1}^{\nu_f} x_i^{(f)} (\sigma_i^{(f)})^3$ is the third moment of the probability distribution $P(\sigma_i^{(f)}) = x_i^{(f)}$, with $x_i^{(f)} \equiv N_i^{(f)}/N^{(f)}$ being the molar fraction of species i. The degree of size-polydispersity of the matrix of fixed hard spheres is quantified by the polydispersity parameter Δ, defined in terms of the first and second moments of $P(\sigma_i^{(f)})$ as

$$\Delta = \frac{\sqrt{\overline{\sigma^{(f)^2}} - \overline{\sigma^{(f)}}^2}}{\overline{\sigma^{(f)}}}. \tag{2}$$

For a given model porous matrix (i.e., given $\sigma_i^{(f)}$ and $x_i^{(f)}$ for $i = 1,2,\ldots,\nu_f$, and $n^{(f)}$), we can consider an adsorbed fluid with given parameters ($n^{(m)} \equiv N^{(m)}/V$ and $\sigma^{(m)}$). We then are primarily interested in identifying a criterium that predicts the conditions under which the mobile particles will loose their mobility due to the confinement imposed by the matrix and/or to the crowding enhanced by the interaction between mobile particles. This immobilization of the fluid particles will occur at a localization-transition surface in the state space of the system, and it is this surface that we would like to determine. Before addressing this problem in its most general case, however, let us start with the limit in which the interactions between the mobile particles can be neglected, so that these particles will only be immobilized (or localized) by the severe confinement imposed by the porous matrix.

A. The Lorentz gas limit: Excluded volume theory

To start the analysis, let us consider the model just described in the limit in which the number concentration $n^{(m)}$ of the adsorbed fluid, and hence its volume fraction $\phi^{(m)} = \frac{\pi}{6} n^{(m)}\left[\sigma^{(m)}\right]^3$, is negligible. This corresponds to the so-called Lorentz gas limit. In the context of this limiting model, let us now approach the description of the localization

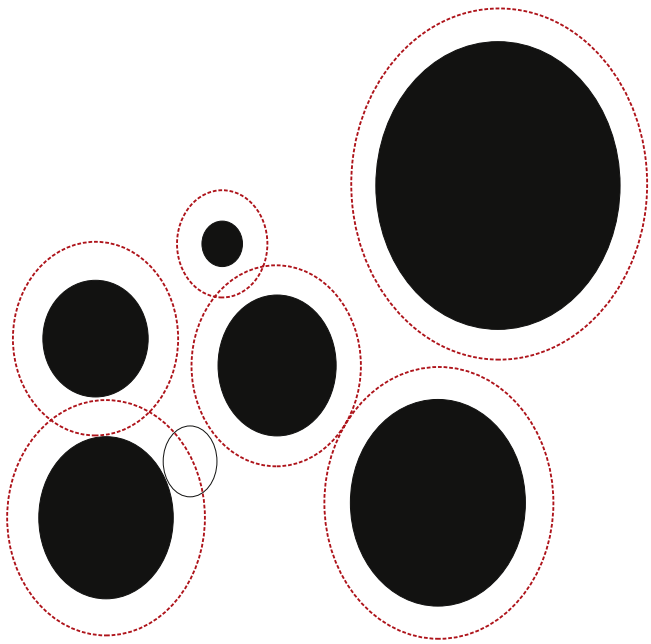

FIG. 1. Random array of fixed spherical obstacles (black circles) with a distribution of diameters, in which a mobile sphere (empty circle) is diffusing. The dotted circles represent the volume inaccessible to the center of this mobile particle.

transition of the non-interacting fluid tracer particles using simple free-volume percolation arguments.

These arguments start by noticing that due to the HS impenetrability and to the finite size $\sigma^{(m)}$ of the tracer fluid particles, an excluded volume $V_i^{(excl)} = \left[\frac{4}{3}\pi(\frac{\sigma_i^{(f)}+\sigma^{(m)}}{2})^3\right]$ exists around each fixed particle of species i, which is inaccessible to the center of the mobile particles, as illustrated in Fig. 1. Neglecting the overlap of the excluded volumes associated with each fixed sphere, the total excluded volume may be written as $V^{(excl)} = \sum_{i=1}^{\nu_f} N_i^{(f)} V_i^{(excl)}$, and the excluded volume fraction $\phi^{(excl)} \equiv V^{(excl)}/V$ can be estimated as

$$\phi^{(excl)} = \phi^{(f)} \left[\frac{\sum_{i=1}^{\nu_f} x_i^{(f)} (\sigma_i^{(f)} + \sigma^{(m)})^3}{\sum_{i=1}^{\nu_f} x_i^{(f)} {\sigma_i^{(f)}}^3} \right]. \tag{3}$$

The excluded volume fraction $\phi^{(excl)}$ is thus the product of two factors, which might be considered as independent control parameters: the volume fraction $\phi^{(f)}$ of the matrix of obstacles and the factor in squared parenthesis, which depends only on the diameter of the mobile particles and on the first three moments of the size distribution $P(\sigma_i^{(f)})$.

The main assumption of these excluded-volume arguments is that the mobility of the fluid tracer particles will decrease as the excluded volume $\phi^{(excl)}$ increases, in such a manner that the mobility vanishes when $\phi^{(excl)}$ reaches a certain critical value $\phi_c^{(excl)}$, corresponding to the conditions in which the free volume $V^{(free)} \equiv V - V^{(excl)}$ ceases to percolate and becomes a set of isolated, non-percolating domains. Rather than attempting to determine the precise value of $\phi_c^{(excl)}$, here, we shall only exploit its very existence and use its value $\phi_c^{(excl)}$ as an arbitrary or adjustable parameter; for the time being, we arbitrarily set $\phi_c^{(excl)} = 0.8$.[36]

In this manner, the equation that determines the critical conditions for the localization of the fluid particles can be written as an expression for the critical value $\phi_c^{(f)}$ of the volume fraction of obstacles at which the fluid particles become immobilized, for a given size distribution of the fixed spheres and a given diameter of the mobile particles. This equation reads

$$\phi_c^{(f)} = 0.8 \times \left[\frac{\sum_{i=1}^{\nu_f} x_i^{(f)} {\sigma_i^{(f)}}^3}{\sum_{i=1}^{\nu_f} x_i^{(f)} (\sigma_i^{(f)} + \sigma^{(m)})^3} \right]. \tag{4}$$

As a simple illustrative application, let us consider a bi-disperse porous matrix (i.e., $\nu_f = 2$) formed by fixed hard spheres of diameters $\sigma_1^{(f)} = (1-\varepsilon)\overline{\sigma^{(f)}}$ and $\sigma_2^{(f)} = (1+\varepsilon)\overline{\sigma^{(f)}}$, with $\epsilon \in [0,1]$, present at equal molar fractions, $x_1^{(f)} = x_2^{(f)} = 0.5$ (see Fig. 2(a)). Under these conditions, Eq. (2) implies that $\Delta = \varepsilon$ and thus, Eq. (4) may be written as

$$\phi_c^{(f)}(\Delta) = \frac{0.8(1+3\Delta^2)}{(1+\sigma^*)[(1+\sigma^*)^2+3\Delta^2]}, \tag{5}$$

where $\sigma^* \equiv \sigma^{(m)}/\overline{\sigma^{(f)}}$. This function is plotted as the solid line of Figs. 2(b)-2(d), corresponding to $\sigma^* = 1-\varepsilon, 1$, and $1+\varepsilon$, respectively.

The solid lines in these figures illustrate the main product of the simple free-volume arguments leading to Eq. (4) above. Each one of these figures can be viewed as a dynamical arrest diagram, which separates the region of the $(\Delta, \phi^{(f)})$ parameter space in two dynamically different phases, namely, one in which the fluid particles are expected to remain delocalized (below the solid line) and another in which these particles are trapped in the unconnected voids between the fixed particles (above the solid line). Thus, the solid line itself is the localization transition line. The specific results in Figs. 2(b)-2(d) are meant primarily to exhibit the kind of information that can be generated by these simple free-volume percolation arguments. Their specific qualitative features, however, are also interesting by themselves.

Thus, intuitively one expects that the localization-delocalization transition must depend significantly on the size of the mobile species relative to a length scale associated to the porous matrix, for example, the mean size of the matrix particles, and the results in Figs. 2(b)-2(d) illustrate the predictions of this theory regarding such dependence. For example, the effect of polydispersity is predicted to be more dramatic when the diameter of the fluid particles is smaller than the mean diameter of the obstacles, as illustrated by Fig. 2(b), which also implies that a more polydisperse matrix requires a higher volume fraction to trap small tracer particles ($\sigma^{(m)} < \overline{\sigma^{(f)}}$). This tendency, however, becomes less apparent as the size of the mobile particles $\sigma^{(m)}$ becomes comparable to $\overline{\sigma^{(f)}}$, as seen in Fig. 2(c). For still larger mobile particles, $\sigma^{(m)} > \overline{\sigma^{(f)}}$, illustrated by the results in Fig. 2(d), the critical volume fraction $\phi_c^{(f)}$ seems to be almost independent of polydispersity, at least in comparison with the situation displayed in Fig. 2(b). In a closer look, however, one observes in Fig. 2(d) a non-monotonic dependence of $\phi_c^{(f)}$ on Δ, indicating a mild but well-defined reentrance, amplified in the inset of Fig. 2(d). Features like this reentrance may

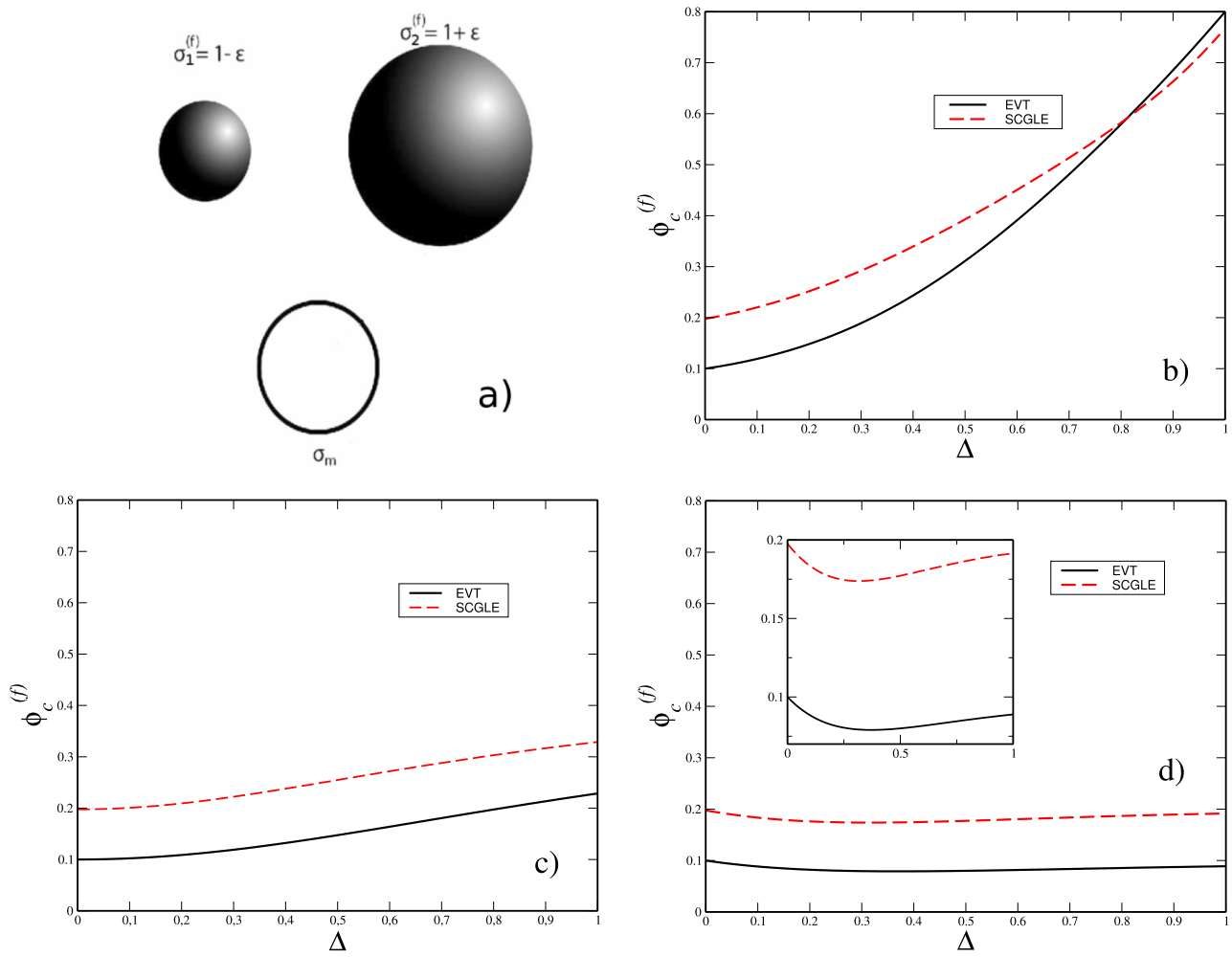

FIG. 2. (a) Schematic size-relationship between the two species of fixed (dark) spheres and the mobile (empty) particles. (b)-(d): Percolation diagrams for a bidisperse and equimolar porous matrix using EVT and SCGLE for (b) $\sigma^* = 1-\varepsilon$, (c) $\sigma^* = 1$, and (d) $\sigma^* = 1+\varepsilon$.

reflect a genuine and interesting subtle effect, not understood in a simple and straightforward pictorial fashion. It, however, could also be just an irrelevant artifact of the oversimplified arguments behind the excluded volume theory. One possible approach to settle this question is to use simulation techniques or alternative, more robust, theories. In this context, let us use this illustrative application to advance an important conclusion regarding the accuracy of these qualitative predictions. We refer to the inclusion in these figures of the dashed lines, corresponding to the results for the localization transition line predicted by the more sophisticated SCGLE theory that we discuss in Sec. III. From the comparison between the solid and the dashed lines in these figures, we conclude that, in spite of the approximations involved in each of these approaches, the general scenario predicted by both theories is essentially identical, a consistency that provides mutual support to their intrinsic qualitative accuracy.

III. THE SCGLE THEORY OF DIFFUSION IN POROUS MEDIA

The simple EVT is particularly useful to construct localization transition diagrams in a simple way under conditions in which the mobility of the fluid particles is only affected by their interactions with the fixed obstacles, but not by the interactions between them, i.e., in the limit in which the number concentration $n^{(m)}$ of the adsorbed fluid is negligible. Let us now introduce an alternative theoretical approach which also allows us to generate the localization transition diagrams in this limit, but which, in addition, will allows us to incorporate the effect of the interactions between mobile particles. As mentioned in the Introduction, a rigorous approach was developed by Krakoviack[13] as a reformulation of mode coupling theory for quenched annealed mixtures. The present approach will be based, instead, on the multicomponent SCGLE theory of colloid dynamics[29,30] and dynamical arrest[33,34] in equilibrated colloidal mixtures. We propose the adaptation of this theory to the description of the diffusion of a fluid adsorbed in a model porous matrix. In particular, in this section, we introduce the referred SCGLE theory and explain how to adapt it to describe the dynamics of a fluid adsorbed in a porous medium. We then apply the resulting equations to the limiting condition $\phi^{(m)} \to 0$, analyzed in Sec. II within the EVT theory, in order to compare the results of both approaches. The applications in which $\phi^{(m)} \neq 0$ will be considered in Sec. IV.

A. SCGLE theory of the dynamics of colloidal mixtures

The dynamic properties of a colloidal mixture of ν species can be described in terms of the relaxation of the fluctuations $\delta n_\alpha(\mathbf{r},t)$ of the local concentration $n_\alpha(\mathbf{r},t)$ of colloidal particles of species α (=1,2,...,ν) around its bulk equilibrium value n_α. The average decay of $\delta n_\alpha(\mathbf{r},t)$ is described by the ISFs $F_{\alpha\beta}(k,t) \equiv \langle \delta n_\alpha(\mathbf{k},t)\delta n_\beta(-\mathbf{k},0)\rangle$ for the Fourier transform $\delta n_\alpha(\mathbf{k},t) \equiv (1/\sqrt{N_\alpha}) \sum_{i=1}^{N_\alpha} \exp i\mathbf{k}\cdot\mathbf{r}_i^{(\alpha)}(t)$ of the fluctuations $\delta n_\alpha(\mathbf{r},t)$. Also, the *self*-component of $F_{\alpha\beta}(k,t)$ (usually referred as the *self*-intermediate scattering function) is defined as $F^{(s)}_{\alpha\beta}(k,t) \equiv \delta_{\alpha\beta}\langle \exp i\mathbf{k}\cdot\Delta\mathbf{r}^{(\alpha)}(t)\rangle$, where $\Delta\mathbf{r}^{(\alpha)}(t) \equiv \mathbf{r}^{(\alpha)}(t) - \mathbf{r}^{(\alpha)}(0)$ is the displacement of any of the N_α particles of species α over a time t and $\delta_{\alpha\beta}$ is the Kronecker's delta function.

Let us denote, for simplicity, the $\nu\times\nu$ matrix $F(k,t)$, with elements $F_{\alpha\beta}(k,t)$, just as $F(t)$ and similarly for the *self*-component. The multi-component version of the SCGLE[30–33] consists of a set of coupled approximate time-evolution equations for $F(t)$ and $F^{(s)}(t)$ which, according to Eqs. (2.1)-(2.6) of Ref. 33, read

$$F(z) = \{zI + [I + \lambda(k)\Delta\zeta^*(z)]^{-1}k^2DS^{-1}(k)\}^{-1}S(k), \quad (6)$$

$$F^{(s)}(z) = \{zI + [I + \lambda(k)\Delta\zeta^*(z)]^{-1}k^2D\}^{-1}, \quad (7)$$

where the argument z means Laplace transform (LT) and $S(k)$ is the matrix of partial static structure factors defined as $S_{\alpha\beta}(k) \equiv \langle \delta n_\alpha(\mathbf{k},0)\delta n_\beta(-\mathbf{k},0)\rangle$. In these equations, I, $\lambda(k)$, $\Delta\zeta^*$, and D are $\nu\times\nu$ diagonal matrices, I being the identity, $D_{\alpha\beta} \equiv \delta_{\alpha\beta}D^0_\alpha$, where D^0_α is the *short-time* self-diffusion coefficient of species α, $\lambda_{\alpha\beta}(k) \equiv \delta_{\alpha\beta}[1 + (k/k_c^{(\alpha)})^2]$, with $k_c^{(\alpha)} \equiv 1.545(2\pi/\sigma_\alpha)$. The matrix $\Delta\zeta^*(t)$ is a diagonal matrix whose αth diagonal element $\Delta\zeta^*_\alpha(t)$ is the time dependent friction function of particles of species α given by

$$\Delta\zeta^*_\alpha(t) = \frac{D^0_\alpha}{3(2\pi)^3}\int d^3k\; k^2[F^{(s)}(t)]_{\alpha\alpha} \times [c\sqrt{n}F(t)S^{-1}\sqrt{n}h]_{\alpha\alpha}, \quad (8)$$

with the elements of the k-dependent matrices h and c being the Fourier transforms $h_{\alpha\beta}(k)$ and $c_{\alpha\beta}(k)$ of the Ornstein-Zernike total and direct correlation functions, respectively, and with the matrix $\sqrt{n}$ defined as $[\sqrt{n}]_{\alpha\beta} \equiv \delta_{\alpha\beta}\sqrt{n_\alpha}$. Here, n_α denotes the number density of species α and h and c are related to S by $S = I + \sqrt{n}h\sqrt{n} = [I - \sqrt{n}c\sqrt{n}]^{-1}$.

Although these equations look rather involved, mostly due to their matrix character, they can be solved numerically using standard methods, to get the full time-dependence of the properties involved. If, however, one is only interested in the long-time asymptotic limit of these properties, the best is to write the asymptotic limit of these equations, leading to the so-called bifurcation equations (Eqs. (5.7)-(5.9) of Ref. 33), the most important of which refers to the equation for $\Delta\zeta^{*(\infty)}_\alpha \equiv \lim_{t\to\infty}\Delta\zeta^*_\alpha(t)$. This equation reads

$$\frac{1}{\gamma_\alpha} = \frac{1}{3(2\pi)^3}\int d^3k\; k^2\{[I + k^2\gamma\lambda^{-1}(k)]^{-1}\}_{\alpha\alpha} \times [c\sqrt{n}\{I + k^2\gamma\lambda^{-1}(k)S^{-1}(k)\}^{-1}\sqrt{n}h]_{\alpha\alpha}, \quad (9)$$

where $\gamma_\alpha \equiv D^0_\alpha/\Delta\zeta^{*(\infty)}_\alpha = \lim_{t\to\infty}\langle(\Delta\mathbf{r}^{(\alpha)}(t))^2\rangle$ is the long-time value of the MSD of species α, which must be infinite if the particles of species α diffuse and must be finite if that species is arrested. In the latter case, $\sqrt{\gamma_\alpha}$ is the localization length of the particles of that arrested species. This provides a practical tool to predict whether a colloidal system should be expected to equilibrate in an ergodic state or will be trapped in an arrested state, given the matrix of equilibrium static structure factors and the short-time self-diffusion coefficient D^0_α of each species ($\alpha = 1,2,\ldots,\nu$), which are the only external inputs needed to solve Eq. (9) for γ_α. Notice that artificially setting $D^0_{\alpha^o} = 0$ for a given species α^o, as we shall soon do to model a species of immobilized obstacles, amounts to setting $\gamma_{\alpha^o} = 0$ for that species.

B. Application to a colloidal fluid diffusing through a porous matrix

Following previous work of our group,[32] let us explain how to use this theory of colloid dynamics in mixtures, as a theory to describe the dynamics of a (generally multicomponent) fluid adsorbed in a porous matrix of fixed spherical objects. To see this, we notice that the other important input of the SCGLEs of Sec. III A are the short-time self-diffusion coefficient D^0_α of each species $\alpha = 1,2,\ldots,\nu$. This is the diffusion coefficient that describes the motion of these particles between collisions, so that if we set $D^0_\alpha = 0$, it means that the particles of species α are assumed not to diffuse in any time scale, i.e., to remain fixed in space. Hence, we may consider the particular application of the previous equations in which for a subset of ν_m species, let us say, $\alpha = 1,2,\ldots,\nu_m$, we have $D_\alpha \neq 0$, whereas for the other $\nu_f = (\nu - \nu_m)$ species ($\alpha = (\nu_m + 1),(\nu_m + 2),\ldots,(\nu_m + \nu_f)$), we arbitrarily set $D_\alpha = 0$. This corresponds to a colloidal mixture of ν_m species of mobile particles diffusing through a porous matrix formed by the ν_f species of artificially immobilized particles. In this paper, we shall only consider the case of a monodisperse adsorbed fluid ($\nu_m = 1$) in a polydisperse matrix ($\nu_f > 1$).

Before using the SCGLEs (6)-(8) to calculate the time-dependent dynamical properties or Eq. (9) to track the immobilization scenarios of the colloidal probes in porous media (and thus draw localization or dynamic arrest diagrams), we must establish the protocol that generates the porous matrix. In this context, two types of such protocols are commonly referred to in the literature, involving, respectively, a quenched annealed (QA) mixture[37,38] and an equilibrated mixture (EM).[10,11] For simplicity, in this paper, we shall only refer to the latter, which consists of considering a $(1 + \nu_f)$-component colloidal mixture in thermal equilibrium and then freezes the motion of the ν_f species that constitute the porous matrix, while letting the remaining species to remain mobile. As discussed in Ref. 32, however, there are no fundamental barriers to consider the QA protocol.

Thus, we proceed as follows. We obtain the static structure factors of the $(1 + \nu_f)$-component HS equilibrated colloidal mixture from the solution of the Ornstein-Zernike integral equation within the Percus-Yevick approximation, analytically determined by Baxter.[39] Given these input static structure factors, we then *arbitrarily* set the short-time self-diffusion

coefficients D_α^0 of the ν_f species ($\alpha = 2, \ldots, \nu_f$) to zero. This implies that $\gamma_\alpha = 0$ for $\alpha = 2, \ldots, \nu_f$, so that we must only solve Eq. (9) for the squared localization length γ_1 of the mobile species. The solution will indicate if the particles of the adsorbed fluid are localized (γ_1 finite) or delocalized ($\gamma_1 \to \infty$). In this way, a systematic application of Eq. (9) for different values of $\phi^{(f)}$ will allow us, for example, to determine the critical value $\phi_c^{(f)}$.

C. Localization transition in the Lorentz gas limit within the SCGLE theory

Let us consider the simplest application of the SCGLE theory just described. This refers to the limit in which we can ignore the interactions between the mobile particles, i.e., the Lorentz gas limit discussed in Subsection II A. We start with the same example of that section, involving a porous matrix formed by a binary mixture ($\nu_f = 2$) of fixed hard spheres of diameters $\sigma_1^{(f)} = (1-\varepsilon)\overline{\sigma^{(f)}}$ and $\sigma_2^{(f)} = (1+\varepsilon)\overline{\sigma^{(f)}}$, with $\epsilon \in [0,1]$, present at equal molar fractions, $x_1 = x_2 = 0.5$. Under these conditions, the solution of Equation (9) leads to the results shown as the dashed lines in Figs. 2(b)-2(d), corresponding to three values of the parameter $\sigma^* \equiv \sigma^{(m)}/\overline{\sigma^{(f)}}$, namely, $\sigma^* = 1-\varepsilon$, 1, and $1+\varepsilon$. As already advanced at the end of Subsection II A, the general scenario predicted by the SCGLE theory is essentially identical to that provided by the simpler excluded-volume theory, a consistency that provides mutual support to the intrinsic qualitative accuracy of both theoretical descriptions.

This simple exercise can be extended in various manners to see the way in which the scenario described by Fig. 2 depends, for example, on the number of species that constitute the matrix, on the probability distribution of diameters (i.e., the molar fractions x_i), etc., and to see if the qualitative agreement between the EVT and the SCGLE theories is preserved under such wider variety of conditions. To see this, we may consider now more complicated porous matrices varying, for example, the number of species of fixed particles ($\nu_f = 2, 3$, and 7) and/or the molar distribution (flat, $P(\sigma_i^{(f)}) = x_i^{(f)} = 1/\nu_f$, or binomial, $P(\sigma_i^{(f)}) = x_i^{(f)} = \nu_f!/[2^{\nu_f} i!(\nu_f - i)!]$), as well as the parameter σ^*.

Thus, using again Eq. (9) and considering all these different possibilities for a given porous matrix, we obtain the corresponding percolation diagrams which are shown in Figs. 3(a)-3(c). In agreement with our previous findings summarized in Figs. 2(b)-2(d) (also displayed as solid lines

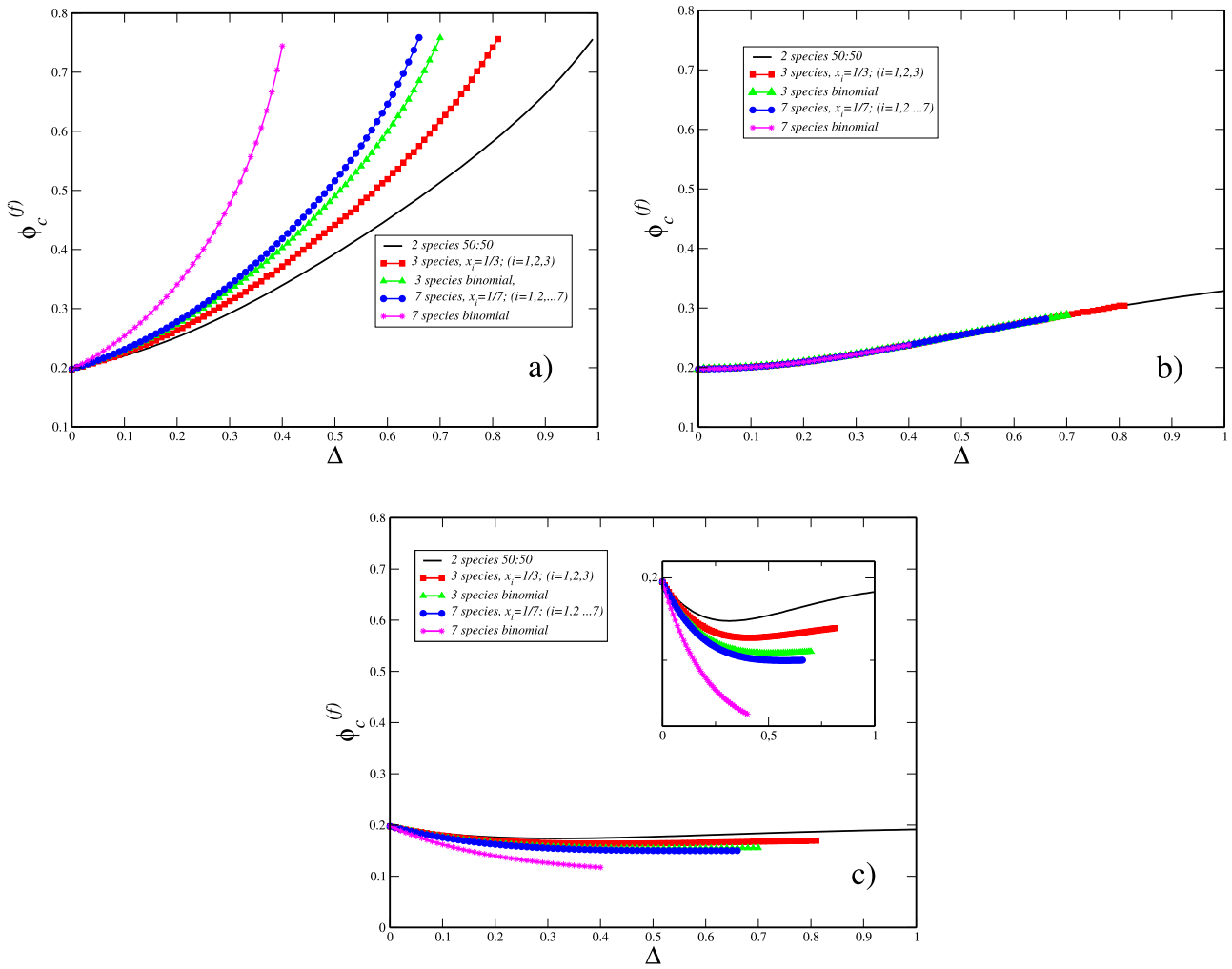

FIG. 3. Percolation diagrams obtained with Eq. (9) for (a) $\sigma^* = 1-\epsilon$, (b) $\sigma^* = 1$, and (c) $\sigma^* = 1+\epsilon$, for porous matrices generated with different number of species and molar distributions.

in Figs. 3(a)-3(c)), the percolation threshold of each matrix is predicted to be dependent on both the polydispersity degree, Δ, and the parameter σ^* which describes the ratio of two characteristic length scales involved. For example, fixing σ^* at $\sigma^* = 1 - \epsilon$, we may determine $\phi_c^{(f)}(\Delta)$ for different porous matrix realizations. Our results are shown in Fig. 3(a). From this figure, we observe that the percolation threshold of each matrix is also a monotonic increasing function of Δ, with a growth rate that also depends on the number of species and on the size distribution. Hence, in this case, a more polydisperse and complex matrix requires a higher volume fraction to localize the tracer particles. As $\sigma^* \to 1$, this trend is less noticeable and, for the exact condition $\sigma^* = 1$, all the percolation lines corresponding to different realizations of the porous matrix surprisingly collapse in the same, mildly monotonically increasing curve of Fig. 2(c), as shown here in Fig. 3(b). Finally, for $\sigma^* = 1 + \epsilon$, the dependence of $\phi_c^{(f)}$ on Δ is displayed in Fig. 3(c). Here, we find that, as already observed in Fig. 2(d), for the binary case, the percolation threshold $\phi_c^{(f)}$ appears to be almost independent on polydispersity, exhibiting, however, an almost unnoticeable reentrance. As illustrated by this figure, such reentrance is more apparent as we increase the number of species, a feature amplified in the inset of the figure.

Let us stress that the range of values for Δ for each percolation curve in this figure is restricted by Eq. (2), which provides an explicit relationship between Δ and ϵ that also depends on both ν_f and $P(\sigma_i^{(f)})$. To clarify this fact in more detail, let us consider a particular example. A 7-component porous matrix may be generated with a random distribution of fixed hard spheres with diameters given by $\sigma_i^{(f)} = \left[1 + \frac{(4-i)}{3}\epsilon\right]\overline{\sigma^{(f)}}$, where $i = 1, 2, \ldots, 7$. Assuming, for example, that this matrix has a binomial size distribution, it is easy to show from Eq. (2) that $\Delta = \epsilon/\sqrt{6} \simeq 0.41\epsilon$. Given that ϵ must be restricted to the interval $0 < \epsilon < 1$, it follows that $0 < \Delta < 0.41$.

To see if all the conclusions drawn from the results in Fig. 3 may be also arrived at using our excluded volume arguments, we may go back to Eq. (4) to compute $\phi_c^{(f)}(\Delta)$ for each case considered above. Our results, displayed in Figs. 4(a)-4(c), show that the physical scenario described by the EVT approach is qualitatively identical to that predicted by the SCGLE approach. One advantage of the simple analytic expression for $\phi_c^{(f)}(\Delta)$ in Eq. (4) is the possibility to explain analytically interesting scaling rules such as that emerging when the condition $\sigma^* = 1$ holds exactly, leading to the collapse of all the transition lines in a single master curve, as already seen in Figs. 3(b) and 4(b). Thus, let us notice that this feature might

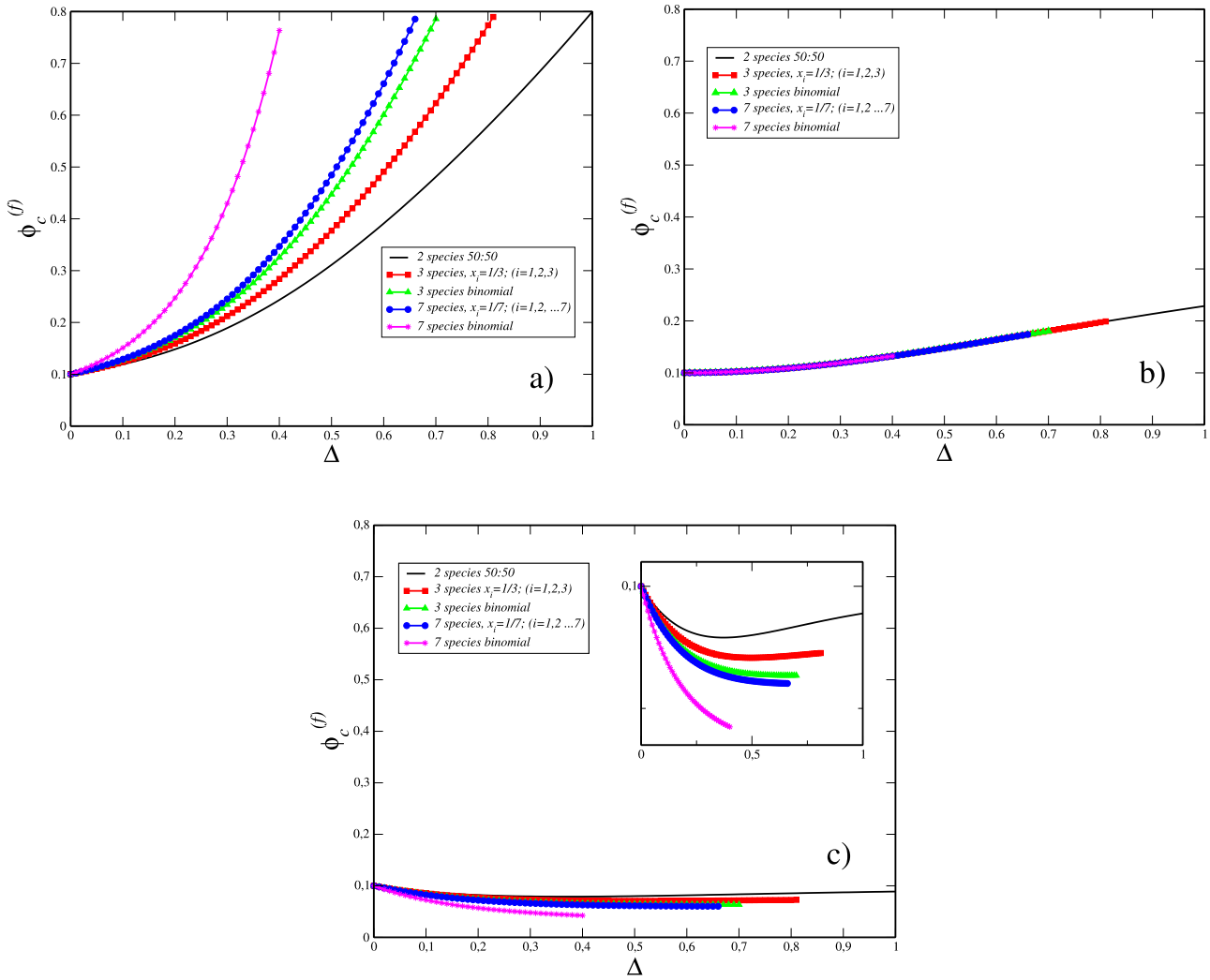

FIG. 4. Percolation diagrams obtained with EVT for (a) $\sigma^* = 1 - \epsilon$, (b) $\sigma^* = 1$, and (c) $\sigma^* = 1 + \epsilon$, for porous matrices generated with different number of species and molar distributions, similar to Fig. 3.

have been anticipated from Eqs. (4) and (5). In fact, starting from the former, it is easy to show that $\phi_c^{(f)}$, as a function of Δ and σ^*, is invariant under changes in the number of species, ν_f, and/or the size distribution, $P(\sigma_i^{(f)}) = x_i^{(f)}$. Hence, the effects induced by ν_f and $x_i^{(f)}$ are contained only in the parameter σ^*, or more precisely, on the specific relationship $\Delta(\epsilon)$. In the particular case $\sigma^* = 1$, Eq. (5) becomes independent on ν_f and x_i, and hence, one would expect the collapse of all the curves.

The main drawback of the simple EVT arguments, however, is the difficulty to extend them away from the *Lorentz gas* limit, an extension needed to describe the effects of the interactions between the mobile particles on their diffusivity and on their localization transition. For this reason, we introduced and implemented the more robust and elaborated SCGLE theory.

IV. ERGODIC AND NON-ERGODIC STATES OF THE ADSORBED FLUID

We now move away from the Lorentz gas limit, $n^{(m)} \to 0$, to consider the simultaneous influence of crowding and confinement as driving factors for the localization of the mobile species. For this purpose, we may use again Eq. (9), this time to scan the full state space of a given fluid embedded in a porous matrix in order to determine the transition line separating the region of (ergodic) fluid states ($\gamma_1 = \infty$) from those (non-ergodic) dynamically arrested (finite γ_1). The localization length $\sqrt{\gamma_1}$ is the dynamic order parameter that indicates if a given point in the state space lies in one region or in the other. The value of γ_1 depends on the ratio $\sigma^* \equiv \sigma^{(m)}/\sigma^{(f)}$ and on the parameters that span the state space, namely, the volume fractions $\phi^{(m)}$ and $\phi^{(f)}$ of, respectively, mobile and fixed hard spheres, the size-polydispersity parameter Δ, the number ν_f of species of fixed particles, and their molar fractions $x_i^{(f)}$. To simplify the present discussion, however, here we shall restrict ourselves to the simplest case in which the matrix is an equimolar binary mixture ($\nu^{(f)} = 2$, $x_1^{(f)} = x_2^{(f)} = 0.5$), so that $\gamma_1 = \gamma_1(\phi^{(m)}, \phi^{(f)}, \Delta, \sigma^*)$. Thus, for a fixed value of σ^*, the dynamical arrest transition surface is embedded in the three-dimensional space $(\phi^{(m)}, \phi^{(f)}, \Delta)$, whose intersection with the plane $\phi^{(m)} = 0$ are the solid lines in each of the three panels of Fig. 2 (corresponding to the three values of the parameter σ^* discussed there). To complement this limiting description of the dynamical arrest surface, let us exhibit now its intersection with the planes $\Delta = 0.0, 0.3, 0.5, 0.6$, and/or 0.7. This is done in Figs. 5(a)-5(c) for, respectively, $\sigma^* = 1 - \epsilon$, 1, and $1 + \epsilon$.

According to Figs. 5(a) and 5(b) (that is, for $\sigma^* \leq 1$), the polydispersity of the matrix increases the ergodic region in the state space in comparison with the limiting case $\Delta = 0$

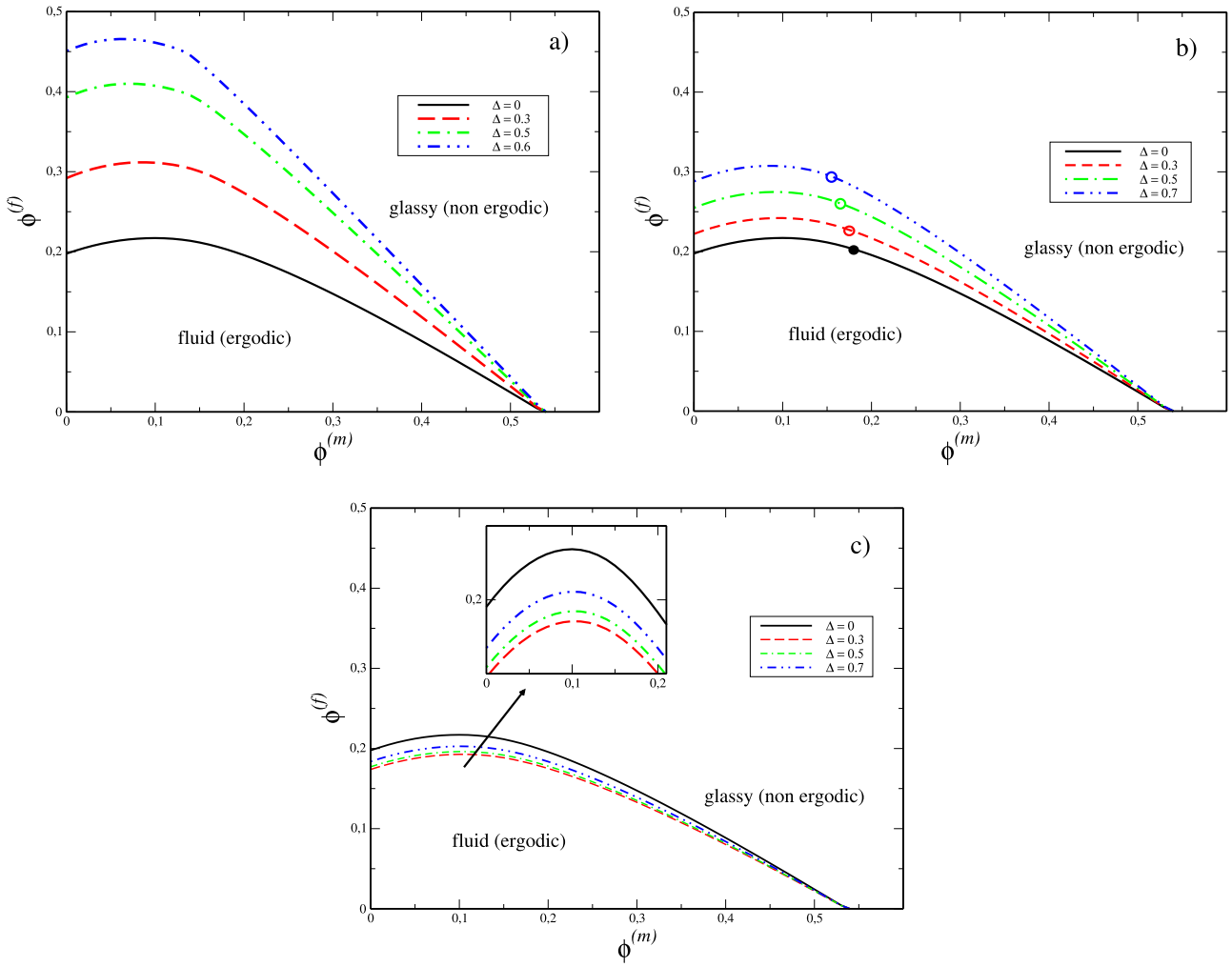

FIG. 5. Dynamical arrest diagrams obtained with SCGLE for a 50 : 50 molar distributed bidisperse matrix for (a) $\sigma^* = 1 - \epsilon$, (b) $\sigma^* = 1$, and (c) $\sigma^* = 1 + \epsilon$.

(solid line). Notice that a quantitative measure of this effect is provided by the value $\phi_c^{(f)}$ at which the transition line intercepts the vertical axis $\phi^{(m)} = 0$ (corresponding to the *Lorentz gas* limit). Clearly, $\phi_c^{(f)}$ increases more strongly with Δ for $\sigma^* = 1 - \epsilon$ (Fig. 5(a)) than for $\sigma^* = 1$ (Fig. 5(b)). This, however, was already revealed by the excluded volume arguments discussed in Subsection II A (see Figs. 2(a) and 2(b)). In fact, in the same discussion, the possibility that this trend could be reversed was already anticipated in Fig. 2(c) for $\sigma^* = 1 + \epsilon$. Such tendency, enhanced in the inset of Fig. 2(c), is now displayed in the dynamical arrest transition lines in Fig. 5(c): contrary to what happens in Figs. 5(a) and 5(b), when polydispersity increases, the fluid region first shrinks (the transition line moves down), but this trend is reversed at larger values of Δ (for which the transition line now moves up). Although this feature may have a limited practical relevance, due to its rather small magnitude, it does illustrate the capability of the SCGLE theory to extend the discussion initiated in the Lorentz gas limit with simple excluded volume arguments (Sec. II) to the full $(\phi^{(m)}, \phi^{(f)}, \Delta, \sigma^*)$ state space.

Let us now refer to another qualitatively relevant generic feature of the dynamical arrest lines displayed in Figs. 5(a)-5(c). We refer to their general shape (i.e., to the dependence of $\phi_c^{(f)}$ on $\phi^{(m)}$), which starts in the Lorentz gas limit at the localization point $(\phi_c^{(m)}, \phi_c^{(f)}) = (0, \phi_c^{(f)})$ and ends at the glass transition point $(\phi_c^{(m)} = 0.537, 0)$, exhibiting the localization-delocalization-localization reentrance whose significance has been discussed, for example, in Ref. 11. These transition lines describe two fundamentally different dynamical arrest mechanisms: near the Lorentz gas regime, they describe a localization transition, only due to the severity of the confinement imposed by the porous matrix. In the opposite regime, at small concentration of obstacles, they correspond to an extension of the bulk HS glass transition, only due to the inter-particle interactions (crowding). This means that somewhere between these two limiting conditions, the dynamical arrest transition changes its nature from localization to glass transition. As an illustration, in Fig. 5(b), we denote by a solid circle in the solid line of Fig. 5(b) the point at which this happens, which corresponds to $\Delta = 0$ and $\sigma^* = 1$, the case considered by Krakoviack[13] in his pioneering discussion of this higher-order singularity.

To identify this singular point, one has to analyze the proper dynamic order parameter, which in the SCGLE theory is the squared localization length γ. Thus, to determine which portion of the transition lines corresponds to a *glass* transition and which portion describes a *localization* transition, we solve Eq. (9) in the vicinity and along each of the transition lines in Figs. 5(a)-5(c). For example, in Fig. 6, we show the result of these calculations performed along the vertical arrows indicated in the inset of the figure for the particular case $\Delta = 0$ and $\sigma^* = 1$. In the main panel, we plot γ^{-1} as a function of $\phi^{(f)}$ at fixed $\phi^{(m)}$, for the indicated sequence of values of $\phi^{(m)}$. These results reveal two qualitatively different patterns in the dependence of γ on $\phi^{(f)}$. In the first of them, illustrated by the arrow at $\phi^{(m)} = 0.3$, γ is infinite (i.e., $\gamma^{-1} = 0$) for $\phi^{(f)} \le \phi_c^{(f)}$, *jumping discontinuously* (dotted line) to a finite value at the critical volume fraction $\phi_c^{(f)}$, and remaining finite for $\phi^{(f)} \ge \phi_c^{(f)}$. This means that the mobile particles remain

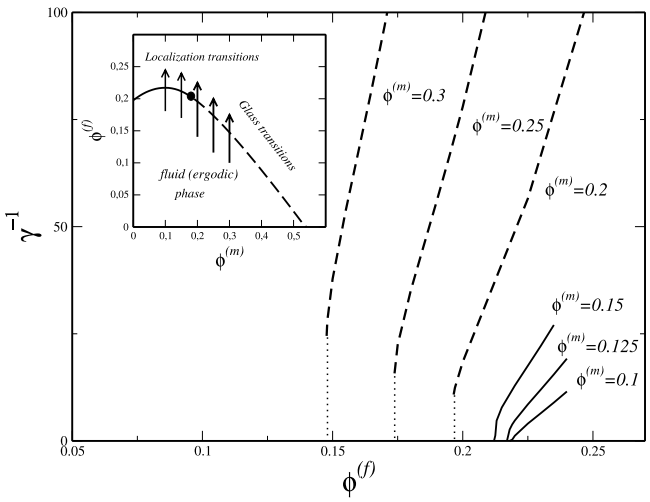

FIG. 6. Behavior of the ergodicity parameter, γ^{-1}, along the two distinct transition lines for the particular case $\Delta = 0$ and $\sigma^* = 1$. The three dotted lines on the left represent type *B* transitions, where γ^{-1} changes discontinuously from zero to a finite value when the system is brought from the fluid (ergodic) region to the glassy state as indicated in the inset. The three solid lines on the right represent type *A* transitions, where γ^{-1} changes continuously from zero to a finite value. Both transition lines meet at the solid circle indicated in the inset.

mobile when the volume fraction of obstacles is smaller than the critical value $\phi_c^{(f)}$ (which depends on $\phi^{(m)}$) and becomes arrested for $\phi^{(f)} \ge \phi_c^{(f)}$.

The second pattern, illustrated by the arrow at $\phi^{(m)} = 0.1$, is similar, except that the discontinuity in γ disappears, i.e., γ varies *continuously* from its value $\gamma^{-1} = 0$ for $\phi^{(f)} \le \phi_c^{(f)}$ to finite values for $\phi^{(f)} \ge \phi_c^{(f)}$. The point $(\phi_c^{(m)}, \phi_c^{(f)})$ at which these two patterns meet is precisely the solid circle in the solid line of Fig. 5(b), located at $(\phi^{(m)} = 0.2, \phi^{(f)} = 0.18)$ in this illustrative example. In the language of mode coupling theory, the pattern involving a discontinuous jump in γ is referred to as a *type B* transition, whereas the continuous one is referred to as a *type A* transition. The former is typical of the behavior observed in the bulk hard-sphere glass transition, and in our case, it extends from the *bulk fluid* limit $(\phi^{(m)} = 0.537, \phi^{(f)} = 0)$ to the higher-order singularity represented by the solid circle just discussed. The latter (*type A*) transition is driven by the localization of particles in disconnected void domains formed by the matrix of fixed spheres, and it extends from the Lorentz gas localization limit, in our example, the state point $(\phi^{(m)} = 0, \phi_c^{(f)} = 0.198)$, to the same solid circle in Fig. 5(b). Applying this procedure to the other illustrative curves in the same or in other figures, we can determine how the location of this higher-order singularity depends on the other parameters considered in our model. For example, in the same figure, we indicate with empty circles the location of this singularity on the other lines corresponding to different polydispersities of the matrix.

V. DYNAMICAL PROPERTIES OF THE ADSORBED FLUID

Section IV illustrates how the solution of Eq. (9) for the dynamic order parameter γ allows us to generate the

dynamic arrest transition lines that separate the ergodic from the non-ergodic regions in the $(\phi^{(m)}, \phi^{(f)})$ subspace. In fact, the same procedure would allow us to determine the full dynamic arrest transition surface in the full state space. The resulting dynamic arrest diagrams are the most relevant and simplest-to-get product of the SCGLE theory. Let us emphasize, however, that the solution of the complete set of SCGLE coupled equations, Eqs. (6)-(8), provides a detailed description of the most relevant dynamic properties of the adsorbed liquid, such as the MSD $\langle(\Delta\mathbf{r}(t))^2\rangle$ of the mobile particles and the *self*-ISF $F^{(s)}(k,t) \equiv \langle \exp[i\mathbf{k}\cdot\Delta\mathbf{r}(t)]\rangle$, at any point of state space. As it will be shown below, within the SCGLE approach, the two different mechanisms for dynamical arrest previously discussed may also be described in terms of the dependence of these dynamic properties on the control parameters $\phi^{(m)}, \phi^{(f)}$, and Δ, as we approach the dynamic arrest transition surface. Let us stress, however, that at this point, we are only interested in illustrating the potential of our method to describe dynamically arrested states in terms of the referred properties, and hence, in this work, we do not provide an exhaustive exploration of the dynamics of the system in the different regions of state space, but only illustrate separately its dependence on $\phi^{(m)}$, $\phi^{(f)}$, and Δ.

For this, let us consider again a colloidal fluid embedded in a bidisperse and equimolar porous matrix and solve the corresponding SCGLEs for the particular case $\sigma^* = 1 + \epsilon$. Let us first describe the case where the mobility of the embedded fluid is mostly affected by the degree of crowding of the mobile particles. From our previous results, we expect that if we approach the dynamic arrest transition line along a path such as that represented by the state points with fixed values of $\phi^{(f)}$ and Δ indicated in Fig. 7(a), the direct interactions between the particles will drive the system to a conventional discontinuous glass transition. This is the situation illustrated in Fig. 7(b) in terms of the evolution of the temporal relaxation of the self-ISF as we increase $\phi^{(m)}$ at fixed values $\phi^{(f)} = 0.1$ and $\Delta = 0.25$. In units of $[\overline{\sigma^{(f)}}]^{-1}$, the wave vector considered is $k = 7.1$, which lies close to the main peak of the static structure factor. Clearly, the so-called α-relaxation time τ_α of the self-ISF $F^{(s)}(k = 7.1,t)$, defined by the condition $F^{(s)}(k,\tau_\alpha) = 1/e$, increases with the fluid concentration. At this moderate density of obstacles, $F^{(s)}(k,t)$ exhibits the onset of a typical glass transition upon increasing $\phi^{(m)}$, where a well defined plateau in $F^{(s)}(k,t)$ appears discontinuously. This behavior is considered one of the hallmarks of a typical *type B* transition and is qualitatively the same as that predicted for

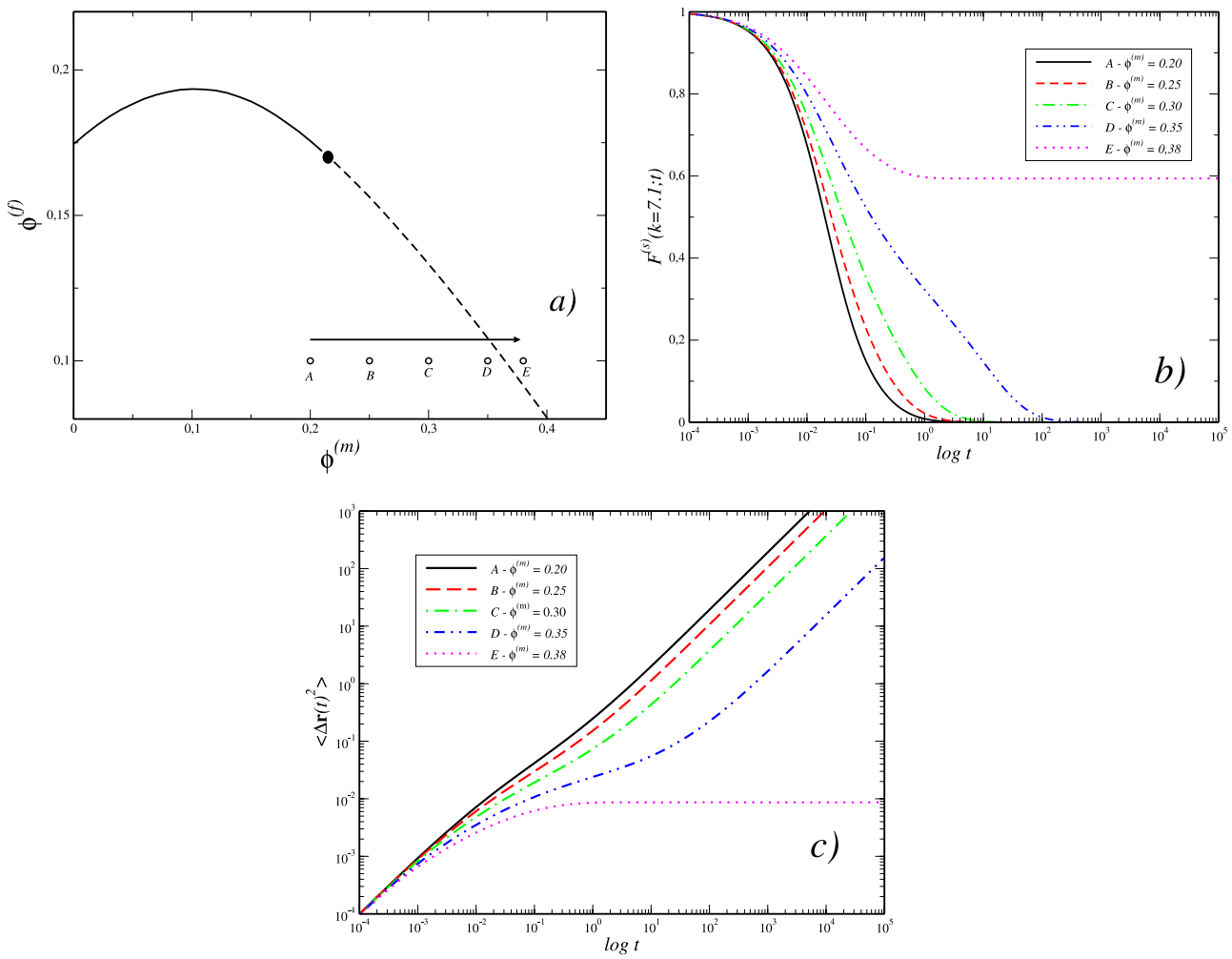

FIG. 7. (a) Dynamical arrest diagram for a fluid embedded in a bidisperse 50:50 molar-distributed porous matrix with fixed values $\sigma^* = 1+\epsilon$ and $\Delta = 0.25$. The state points *A*-*E* represent a path for fixed concentration of obstacles $\phi^{(f)} = 0.1$ and fluid concentrations $\phi^{(m)} = 0.2, 0.25, 0.30, 0.35$, and 0.38, near the glass transition line (dashed). (b) Time-evolution of the *Self*-ISF (k = 7.1) and (c) mean square displacement for the points *A*-*E* along the path displayed in (a).

the *bulk* glass transition (a similar process to that in Fig. 7(a) but at $\phi^{(f)} = 0$), and in general for matrix volume fractions below that of the higher-order singularity represented by the solid circle.[11,12,15,16] To complement these results, in Fig. 7(c), we display the corresponding MSD, where the slowing down of the dynamics is also observed with increasing $\phi^{(m)}$. In qualitative consistency with previous simulation results, for moderate density of obstacles and upon increasing the fluid concentration, the MSD displays an intermediate time regime in which it grows very slowly and, subsequently, becomes diffusive. At even larger $\phi^{(m)}$, the MSD shows a plateau caused by the caging effect, another well known feature of *type B* transitions.

To describe a typical *localization* transition, let us now approach the dynamical arrest transition line by increasing the matrix volume fraction $\phi^{(f)}$ at fixed values $\phi^{(m)} = 0.1$ and $\Delta = 0.25$, as illustrated by the path displayed in Fig. 8(a). In this case, the stronger influence of the structure of the porous matrix changes drastically the nature of the transition. For example, Fig. 8(b) shows the onset of a single step long-tailed relaxation of the corresponding self-ISFs with increasing density of obstacles. Notice that, in this case, the value of the non-ergodicity parameter, $f^{(s)}(k)$, changes continuously. This differs notably from the situation illustrated in Fig. 7(b). The emergence of such *long tail* in the self-ISF's relaxation pattern is considered as one of the typical signatures of the occurrence of a *localization type A* transition.[11,12,15,16] In addition, in Fig. 8(c), we display the behavior of the corresponding MSD. Clearly, in this case, the functional form of the MSD is more sensitive to the obstacle concentration $\phi^{(f)}$ than the situation illustrated in Fig. 7(c) for $\phi^{(m)}$. At densities of obstacles lower than the transition line, one simply observes the expected diffusive behavior ($\langle \Delta \mathbf{r}^2(t) \rangle \sim t$). Upon increasing $\phi^{(f)}$ and approaching this line, the "motion" of the mobile particles deviates from the diffusivity and a subdiffusive regime appears[11,12] ($\langle \Delta \mathbf{r}^2(t) \rangle \sim t^x$, $x < 1$). Finally, one arrives to a critical density at which we observe a clear plateau indicating that the mobile particles cease to percolate and are trapped into the unconnected voids formed by a dense porous matrix. These features may also be interpreted as the hallmarks of a *type A* transition and are also in qualitative agreement with the independent results of Ref. 27.

To describe now the effect of the degree of polydispersity of the porous matrix on the mobility of the embedded fluid,

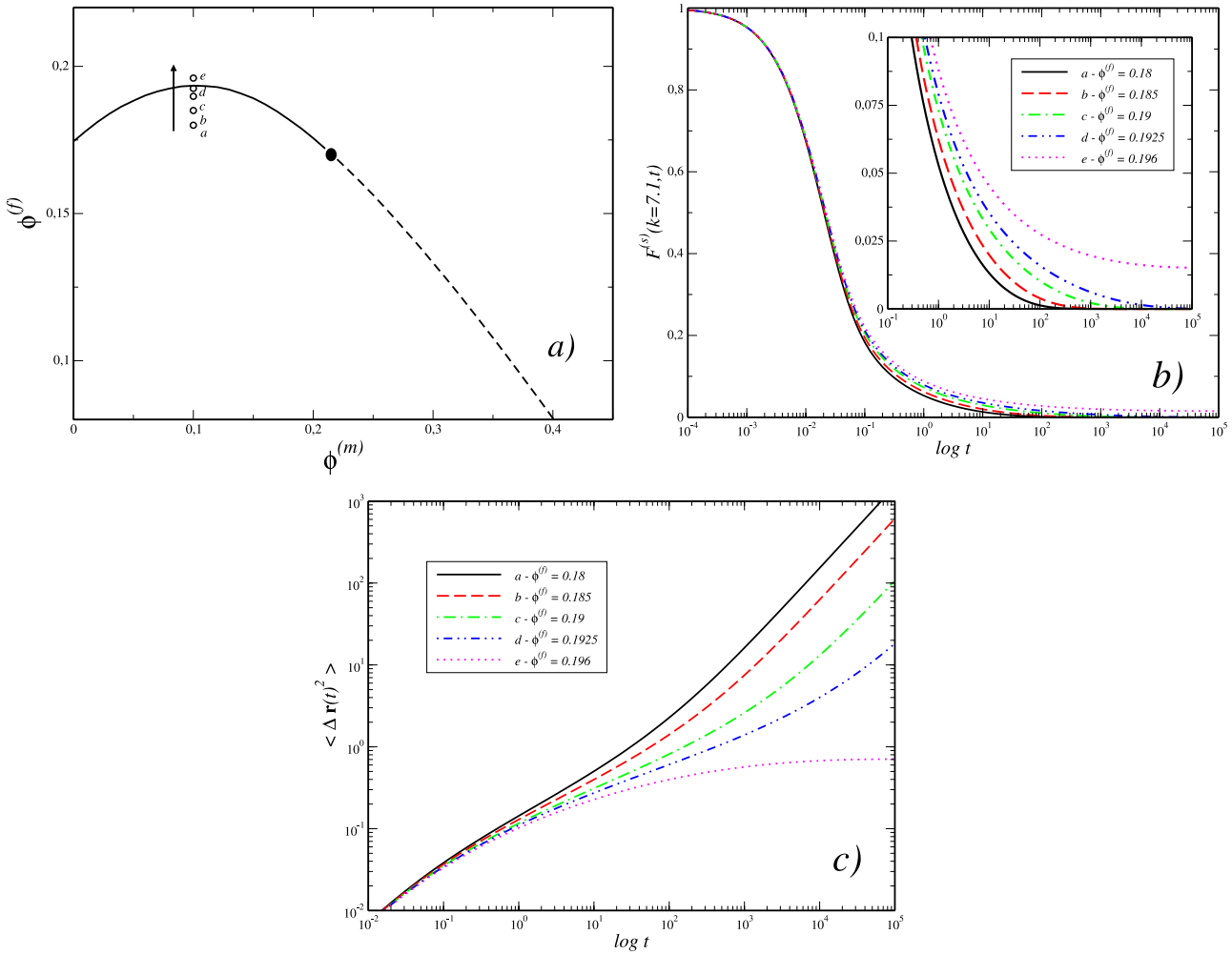

FIG. 8. (a) Dynamical arrest diagram for a fluid embedded in a bidisperse 50:50 molar-distributed porous matrix with fixed values $\sigma^* = 1 + \epsilon$ and $\Delta = 0.25$. The state points *a*-*e* represent a path for constant concentration of fluid $\phi^{(m)} = 0.1$ and obstacle concentrations $\phi^{(f)} = 0.18, 0.185, 0.19, 0.1925$, and 0.196, near the localization transition line (solid). (b) Time-evolution of the *Self*-ISF ($k = 7.1$) and (c) mean square displacement for the points *a*-*e* along the path displayed in (a).

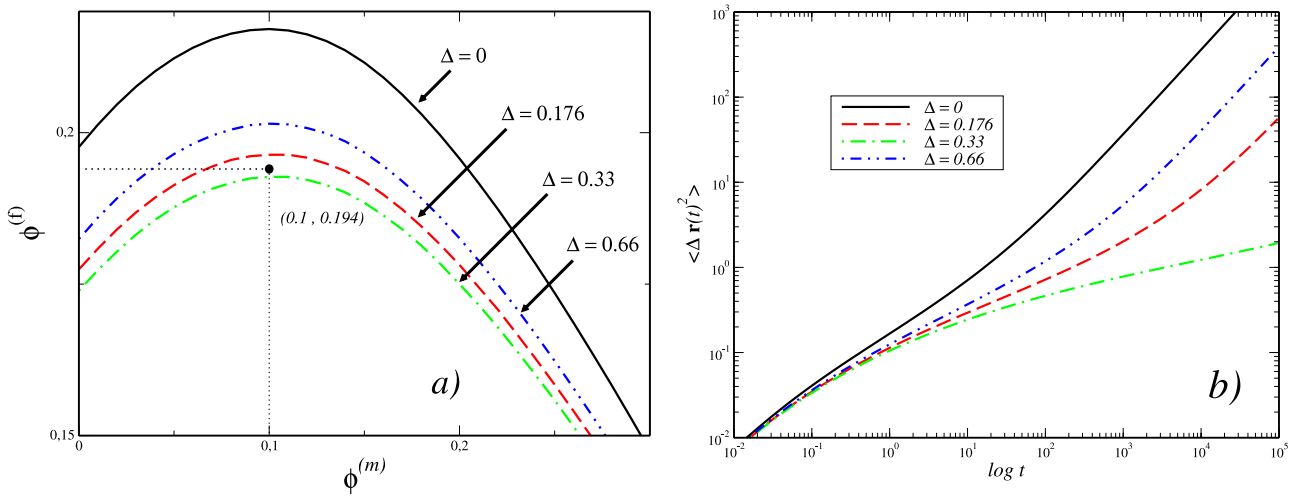

FIG. 9. (a) Dynamical arrest diagrams for a fluid embedded in a bidisperse 50:50 molar-distributed porous matrix with $\sigma^* = 1+\epsilon$ and different values of polydispersity $\Delta = 0, 0.176, 0.33, 0.66$. (b) Mean square displacement for the HS fluid with fixed values $\phi^{(m)} = 0.1$ and $\phi^{(f)} = 0.194$ (solid circle in (a)) as a function of Δ.

let us consider a fixed point in the subspace $(\phi^{(m)}, \phi^{(f)})$ such that, for $\Delta = 0$, this point lies in the fluid region, as shown in Fig. 9(a). By increasing Δ, the transition line first moves downward and eventually "*crosses*" this point leaving it now in the non-ergodic region. A further increase in Δ will move the transition line in the opposite way, "*crossing*" again the fixed point (recall that, accordingly to Fig. 5(c), for $0 < \Delta \lesssim 0.3$, the transition line is predicted to move down, whereas for $\Delta > 0.3$, the transition line is predicted to move up). Thus, intuitively one expects that this procedure will affect the mobility of the embedded fluid in two different and opposite ways: for $\Delta \lesssim 0.3$, the mobility might be hindered by the random network of obstacles, whereas for sufficiently large values of Δ, diffusivity should be restored. Fig. 9(b) confirms nicely these expectations in terms of the MSD of the embedded fluid.

VI. CONCLUSIONS

In this work, we have illustrated the use of the SCGLE theory of the dynamics of colloidal mixtures to describe the dynamical arrest transitions of a monodisperse hard-sphere fluid diffusing through a polydisperse porous matrix. Such porous matrix was modelled as a mixture of fixed HS with a given size distribution, whose translational degrees of freedom were artificially quenched by arbitrarily setting the corresponding short-time self-diffusion coefficients equal to zero. In this contribution, we have focused on the description of some of the most relevant effects induced by the degree of polydispersity of the porous matrix over the dynamical arrest phenomena. In agreement with previous theoretical predictions and results from computer simulations, two different transition scenarios for dynamical arrest where observed: discontinuous *bulk-like* glass transitions for low concentrations of obstacles and continuous *localization-like* transitions at higher concentrations of the porous matrix. Here, however, we systematically illustrated the effects of varying the polydispersity of the porous matrix which were not been studied in any of the previous works.

In the *dilute* regime of the fluid, we proposed a simple excluded volume theory, able to describe how the critical percolation volume fraction $\phi_c^{(f)}$ of the porous matrix depends on the polydispersity parameter Δ. Although this EVT description does not take into account many relevant aspects (for example, direct interactions between the mobile particles or excluded volume overlaps), we found an interesting qualitative consistency between SCGLE and EVT theories in the Lorentz gas limit, providing mutual support to their independent predictions. For example, an interesting behavior for the percolation threshold dependence on Δ was found using both theories given the condition $\sigma^* = 1$, for which all the percolation curves collapse on a master curve, irrespective of the number of species constituting the porous matrix or their molar distribution. This feature, however, can be described by appealing to our excluded volume arguments, suggesting that our EVT may allow us to explain analytically interesting scaling rules.

We found that the localization of the transition line in the state space of the system, separating the fluid (ergodic) states from the dynamically arrested (non-ergodic) states, changes with polydispersity and these changes also depend on the size of the mobile particles. In contrast, the topology of the transition lines is practically independent on Δ, and thus, the reentrance scenario previously found for the EM protocol and also observed even in the absence of polydispersity ($\Delta = 0, \sigma^* = 1$) is preserved. To complement our description of the dynamically arrested states of the embedded fluid, we have used the full SCGLEs to calculate the relevant dynamic properties such as the MSD or the *self*-ISF $F^{(s)}(k,t)$ upon the two dynamical arrest transition lines, exhibiting thus the ability of the SCGLE approach to describe diffusion processes in confined media as well as to distinguish the two different dynamical arrest mechanisms predicted separately by Krakoviack, Kurzidim *et al.*, Kim *et al.*, etc.

Let us mention that, although there are no fundamental barriers within the SCGLE approach to discuss the dynamics of the embedded fluid also in terms of the collective part, $F(k,t)$, of the ISF (not shown here), in this paper, we focused

on *single-particle* properties given the number of separate and independent works where these quantities were extensively calculated with computational simulations[10–12,15,16,27] and which allow us to contrast our results. There is, however, an important aspect concerning to the comparison of our results with some of the previous predictions of MCT for quenched annealed mixtures which must be mentioned. This refers to the decoupling of the self- and collective correlations predicted by the MCT approach,[14] in which an obstacle density domain is observed where the liquid-glass transition is always preceded by a continuous diffusion-localization transition. The results displayed in Sec. V, however, suggest that this scenario is not observed within the SCGLE approach, where $F^{(s)}(k,t)$ displays dynamical arrest only up to the transition line. This difference with MCT is the result of the structure of the SCGLEs in which the matrices $F(k,t)$ and $F_s(k,t)$ defined in Eqs. (6) and (7) are both variables attached to the time-dependent friction functions $\Delta\zeta^*_\alpha(t)$ defined in Eq. (8). Thus, contrary to MCT, where the relevant dynamic order parameters (or non-ergodicity parameters) are the long-time asymptotic values $f_{\alpha\beta}(k)$ of $F_{\alpha\beta}(k,t)/S_{\alpha\beta}(k)$, in the SCGLE theory, the asymptotic values $[\Psi(k)]_{\alpha\alpha} \equiv \lim_{t\to\infty}[F(k,t)S^{-1}(k)]_{\alpha\alpha}$ and their self-components $[\Psi^{(s)}(k)]_{\alpha\alpha} \equiv \lim_{t\to\infty}[F^{(s)}(k,t)]_{\alpha\alpha}$ are both attached to a single scalar dynamic order parameter, namely, the localization length γ_α (see Eq. (9)), which are the inverse of the long-time asymptotic values of $\Delta\zeta_\alpha(t)$. For this reason, if γ_α is infinite, both $[\Psi(k)]_{\alpha\alpha}$ and $[\Psi^{(s)}(k)]_{\alpha\alpha}$ vanish and both $[F(k,t)S^{-1}(k)]_{\alpha\alpha}$ and $[F^{(s)}(k,t)]_{\alpha\alpha}$ decay to zero, and the system is in an ergodic state, whereas if γ_α is finite, both $[\Psi(k)]_{\alpha\alpha}$ and $[\Psi^{(s)}(k)]_{\alpha\alpha}$ are different from zero and both $[F(k,t)S^{-1}(k)]_{\alpha\alpha}$ and $[F^{(s)}(k,t)]_{\alpha\alpha}$ will not decay, and the system will remain in a non-ergodic state.

Thus, the SCGLE theory will never lead to the scenario predicted by MCT involving the existence of regions where $F(k,t)$ decays and $F_s(k,t)$ does not. Of course, only the experimental observations will determine which of the two scenarios (SCGLE vs. MCT) is correct. The discussion of this point, however, must be based on a careful and critical assessment of the experimental and computational evidences and is beyond the scope of this manuscript. Just as it has occurred in the case of monodisperse porous matrices, we expect that the most salient predictions of the present paper will be successfully tested by further simulation experiments.

ACKNOWLEDGMENTS

The authors acknowledge R. Juárez-Maldonado for helpful discussions and raised comments and P. Mendoza-Méndez and E. Lázaro-Lázaro for technical assistance in the numerical solution of the SCGLE equations. This work was supported by the Consejo Nacional de Ciencia y Tecnología (CONACYT, México), through Grant Nos. 182132 and 242364, and by Secretaría de Educación Pública (SEP, México) through Red Física de la Materia Blanda.

[1]R. J. Ellis, Curr. Opin. Struct. Biol. **11**(1), 114 (2001).
[2]R. J. Ellis and A. P. Minton, Nature **425**, 27 (2003).
[3]T. Kühn, T. O. Ihalainen, J. Hyväluoma, N. Dross, S. F. Willman, J. Langowski, M. Vihinen-Ranta, and J. Timonen, "Protein diffusion in mammalian cell cytoplasm," PLoS One **6**(8), e22962 (2011).
[4]K. Luby-Phelps, *International Review of Cytology* (Academic Press, 2000), Vol. 192.
[5]F. D'Orazio, J. C. Tarczon, W. P. Halperin, K. Eguchi, and T. Mizusaki, J. Appl. Phys. **65**, 742 (1989).
[6]S. G. J. M. Kluijtmans, Els H. A. de Hoog, and A. P. Philipse, J. Chem. Phys. **108**, 7469 (1998).
[7]I. C. Kim and S. Torquato, J. Chem. Phys. **96**, 1498 (1992).
[8]M. J. Saxton, Biophys. J. **66**, 394 (1994).
[9]B. J. Sung and A. Yethiraj, J. Chem. Phys. **128**, 054702 (2008).
[10]K. Kim, Europhys. Lett. **61**(6), 790 (2003).
[11]K. Kim, K. Miyazaki, and S. Saito, Europhys. Lett. **88**, 36002 (2009).
[12]K. Kim, K. Miyazaki, and S. Saito, J. Phys.: Condens. Matter **23**, 234123 (2011).
[13]V. Krakoviack, Phys. Rev. Lett. **94**, 065703 (2005).
[14]V. Krakoviack, Phys. Rev. E **79**, 061501 (2009).
[15]J. Kurzidim, D. Coslovich, and G. Kahl, Phys. Rev. Lett. **103**, 138303 (2009).
[16]J. Kurzidim, D. Coslovich, and G. Kahl, Phys. Rev. E **82**, 041505 (2010).
[17]P. R. Van Tassel, Phys. Rev. E **60**, R25(R) (1999).
[18]L. Zhang and P. R. Van Tassel, J. Chem. Phys. **112**, 3006 (2000).
[19]V. Krakoviack, Phys. Rev. E **82**, 061501 (2010).
[20]V. Krakoviack, Phys. Rev. E **84**, 050501(R) (2011).
[21]W. Kob, S. Roldán-Vargas, and L. Berthier, Nat. Phys. **8**, 164167 (2012).
[22]C. Cammarota and G. Biroli, Proc. Natl. Acad. Sci. U. S. A. **109**, 8850 (2012).
[23]S. Karmakar and G. Parisi, Proc. Natl. Acad. Sci. U. S. A. **110**, 2752 (2013).
[24]W. Kob and L. Berthier, Phys. Rev. Lett. **110**, 245702 (2013).
[25]G. Szamel and E. Flenner, Europhys. Lett. **101**, 66005 (2013).
[26]H. van Beijeren and O. Mülken, Phys. Rev. E **71**, 036213 (2005).
[27]F. Höfling, T. Franosch, and E. Frey, Phys. Rev. Lett. **96**, 165901 (2006).
[28]H. van Beijeren, Rev. Mod. Phys. **54**, 195 (1982).
[29]L. Yeomans-Reyna and M. Medina-Noyola, Phys. Rev. E **62**, 3382 (2000).
[30]M. A. Chávez-Rojo and M. Medina-Noyola, Phys. Rev. E **72**, 031107 (2005); **76**, 039902 (2007).
[31]L. Yeomans-Reyna, M. A. Chávez-Rojo, P. E. Ramírez-González, R. Juárez-Maldonado, M. Chávez-Paez, and M. Medina-Noyola, Phys. Rev. E **76**, 041504 (2007).
[32]M. A. Chávez-Rojo, R. Juárez-Maldonado, and M. Medina-Noyola, Phys. Rev. E **77**, 040401(R) (2008).
[33]R. Juárez-Maldonado and M. Medina-Noyola, Phys. Rev. E **77**, 051503 (2008).
[34]R. Juárez-Maldonado, M. A. Chávez-Rojo, P. E. Ramírez-González, L. Yeomans-Reyna, and M. Medina-Noyola, Phys. Rev. E **76**, 062502 (2007).
[35]The reader should notice that our notation differs from that of other authors. In particular, the works of V. Krakoviack and K. Kurzidim *et al.* (see references above) use a similar but inverted notation in which the labels f and m stand, respectively, for *fluid* and *matrix* particles.
[36]Within our excluded volume arguments, $\phi_c^{(excl)}$ is just an arbitrary empirical parameter whose value only shifts the critical arrest line without substantially changing the shape. One might be tempted to use this parameter so that the SCGLE and EVT critical lines match at the monodisperse limit $\Delta \to 0$. Although this procedure might be helpful for a quantitative comparison between both approaches, we did not use it because it leads to the unphysical result $\phi_c^{(excl)} = 1.6$.
[37]M. Schmidt, Phys. Rev. E **66**, 041108 (2002).
[38]M. Schmidt, Phys. Rev. E **79**, 031405 (2009).
[39]R. J. Baxter, Aust. J. Phys. **21**, 563 (1968).